



Numerical investigation of the effect of obstacle shape on deflagration to detonation transition in a hydrogen–air mixture



Ashley M. Coates^{a,b,*}, Donovan L. Mathias^a, Brian J. Cantwell^b

^a NASA Ames Research Center, MS 258-5, Moffett Field, CA 94035, USA

^b Stanford University, Aeronautics and Astronautics, 496 Lomita Mall, Stanford, CA 94305, USA

ARTICLE INFO

Article history:

Received 12 March 2019

Revised 31 July 2019

Accepted 31 July 2019

Keywords:

Combustion

Deflagration

Detonation

Hydrogen

Simulation

ABSTRACT

The potential for deflagration to detonation transition (DDT) in an uncontained failure poses extreme risk to nearby personnel. This study performs numerical simulations with detailed chemistry models of confined stoichiometric hydrogen–air mixtures interacting with flow obstructions to better understand the mechanisms of detonation initiation which will inform future risk assessments. Unique obstacle geometries, including both rectangular and curved obstacles, are considered in an effort to isolate important contributors to DDT. Contributors are shown to be pressure wave interactions in unburned fuel and flow features, such as vortical structures, which encourage flame acceleration. In this study, detonation was only observed in cases with sharp-edged obstacles and not in smooth-walled cases. The sharp edges introduced vortex shedding which contributed to flame distortion and resulted in acceleration. In addition, detonation was observed where strong pressure waves and reflections interacted in unburned fuel. The variations in geometry within the sharp-edged obstacles had some effect on vortex shedding and the reflections of generated shocks resulting in small changes in detonation location, however, the mechanism of DDT appeared the same, and the changes were small in comparison to the smooth-walled cases which did not detonate.

Published by Elsevier Inc. on behalf of The Combustion Institute.

This is an open access article under the CC BY-NC-ND license.

(<http://creativecommons.org/licenses/by-nc-nd/4.0/>)

1. Introduction

The risk to human safety of large, explosive failures as a result of unwanted ignition of a fuel source is important to many different fields from hydrogen storage facilities to mines to rocket propulsion systems. The ignition energy for many of these fuels, like hydrogen, is extremely low, and therefore introduces large risk because a very weak ignition source could lead to a flame that rapidly accelerates and transitions to detonation, significantly risking nearby personnel and equipment. We are interested in the risk posed to crew safety should an uncontained failure occur in a rocket engine bay, as well as understanding the factors contributing to that risk in order to influence the design of safer vehicles. Reliably determining the flame speed, flame location, overpressures, and the potential for transition to detonation is crucial to performing accurate risk assessments for the safety of the crew in this scenario. We will use numerical simulations of hydrogen–air in

a tube to understand the fundamental mechanisms of deflagration to detonation transition (DDT). We can then apply this understanding to future risk assessment studies for more complex scenarios.

Researchers have studied various aspects of flame propagation and the transition from deflagration to detonation in both numerical and experimental studies in an effort to understand the mechanisms associated with DDT. We point readers to the literature [1,2] for detailed summaries of the field. Oran and Gamezo have presented a comprehensive discussion of theoretical and numerical efforts to understand DDT [1], while Ciccarelli and Dorofeev have presented a review focused on the experimental investigations [2]. Here, we will discuss several of the studies that have been conducted. We were particularly interested in configurations involving obstacles, and were performing numerical simulations, so we generally focused on numerical studies of DDT involving obstacles. As more studies have been conducted for different configurations and flow regimes, a few different potential mechanisms for DDT have been proposed. The mechanisms which have been observed may also be parameter dependent so different mechanisms may be active in different cases. Two explanations that appear throughout the literature are the Zeldovich gradient mechanism and the

* Corresponding author at: NASA Ames Research Center, MS 258-5, Moffett Field, CA 94035, USA.

E-mail address: ashley.m.coates@nasa.gov (A.M. Coates).

Shock Wave Amplification by Coherent Energy Release (SWACER) mechanism. The Zeldovich gradient mechanism says that if the temperature in a combustible gas is nonuniform, the gas will expand unevenly, and this can result in shock or detonation waves [3]. Several studies, for example [4,5], have suggested that hot spots in the flow ahead of the flame front created by strong shocks reflecting off of obstacles allow detonation waves to form through the Zeldovich gradient mechanism. The SWACER mechanism [6] says that the chemical energy release and the associated shock wave generated are in phase. This adds strength to the propagating shock. The shock wave and reaction zone can then amplify to a detonation if spatial gradients are appropriate.

Many of the studies on DDT have considered obstructed flows because literature has shown [4,7–9] that the addition of obstacles reduces the time and distance to a potential detonation, making it easier to run experiments and numerical simulations that capture DDT. Gaathaug et al. [10] showed that even one obstacle in the flow can result in transition to detonation. With the addition of obstacles, a number of additional parameters are variable such as size, shape, and placement of obstacles. Teodorczyk et al. [7] conducted experiments with rectangular obstacles in a hydrogen–air environment to determine regimes for deflagrations, transition, and detonations. In these studies, the blockage ratio, distance between obstacles, and the mixture ratio of the gas were varied. The results showed that increasing the blockage ratio decreased the DDT hazard, while increasing the spacing between obstacles with high blockage ratios increased the DDT hazard. In comment on the propagation of the flame, Teodorczyk et al. [7] agreed with observations that the introduction of an obstacle field can rapidly accelerate a flame to high velocities until a terminal, average velocity is reached. These accelerated flames drive pressure waves with large overpressures, a concern in the present work for risk analyses, and can then transition to detonation. In previous experiments with rectangular obstacles and hydrogen–air mixtures, Teodorczyk et al. [11] showed that fast propagation speeds were maintained by intense combustion as a result of flame turbulence amplification.

Heidari and Wen [12] computationally considered a two-dimensional, symmetric, rectangular channel with rectangular obstacles using implicit large eddy simulations (ILES). They worked to develop a numerical approach for modeling flame acceleration and the transition to detonation which captures the various flow regimes. In developing their approach, Heidari and Wen looked at ways to reduce mesh element size for these simulations as well as different chemical reaction models. The spacing between grid points must be small to capture the flow, but the large meshes can be computationally prohibitive. Two methods of reducing the mesh size were considered: adaptive mesh refinement and using multiple grids with different regions refined depending on where the flame and large gradients were located. In [8], Heidari and Wen determined grid spacing should be no larger than 10 microns for their problem and approach based on comparing simulation results at several refinements. This gave 20 points in the detonation half reaction length. In the chemistry modeling discussion [12], both a 1-step and 21-step reaction set were considered. The 21-step chemistry model detonated at a later obstacle than the 1-step model. It was not clear to Heidari and Wen which model was more accurate, however they felt the 1-step model included more tuning to better match individual regimes (laminar, deflagration, detonation, etc.). The 21-step model was derived for one condition. The results of the simulations suggested that increasing the burning surface area increased the energy addition which accelerated the flame. Also, high pressure regions were created where pressure waves reflecting off obstacles and walls interacted, allowing for localized explosions and possibly detonation. Heidari and Wen noted in [8,12] that these results were somewhat different

than what previous numerical studies [4] have shown which explain DDT through the Zeldovich gradient and show DDT occurring in the corner of the obstacles instead of at the flame front above the obstacles as was seen in these studies. The authors concluded the results appeared to be more readily explained by the activity of the SWACER mechanism.

In a study by Gamezo et al. [4], 2D simulations were conducted for a channel with rectangular obstacles in a hydrogen–air mixture. The simulations used a one-step Arrhenius model for chemistry and it was noted that, due to the limitations of the model, only qualitatively correct results were obtained. Blockage ratio remained constant in this work, while the size of the domain and spacing of the obstacles changed. Gamezo et al. discussed the acceleration of the flame as a result of flame surface area increasing, and therefore energy addition rate increasing. Instabilities in the flow and interactions in the obstacle wakes were described as responsible for the flame surface area increase. Transition to detonation in these simulations occurred in the corner of an obstacle when a Mach stem interacted with an obstacle and created a hot spot ahead of the main flame front. Variations in channel size were shown to affect the time and distance to DDT. Gamezo et al. determined that time and distance increased linearly with d^2 , where d is the height of the channel. Continuing to look at rectangular obstacles and spacing, Gamezo et al. [13] considered the effect on DDT of the spacing between obstacles. The results showed that flame acceleration increased as spacing decreased because of the additional flow perturbations which increased flame surface area. Results also showed that larger spacing led to easier DDT because Mach stems had space to form between obstacles. These two competing trends resulted in three regimes of DDT.

Goodwin et al. [5] considered changes in blockage ratio from very small to large, and the effect it had on the DDT mechanisms in both two dimensional and three dimensional simulations of small channels with rectangular obstacles in an ethylene–oxygen mixture. They found that flows with high blockage ratios detonated through the gradient mechanism while flows with intermediate blockage ratios detonated in several different ways including behind Mach reflections, at flame fronts, or from shock focusing. Both gradient of reactivity and SWACER were noted as methods of DDT as blockage ratio varied. Turbulence is also discussed as an important factor in detonation initiation. Overall, they found that increasing the blockage ratio shortened the time and distance to detonation. Relative to the two-dimensional simulations, the three-dimensional simulations also exhibited shorter time and distance to detonation. Goodwin et al. further studied the low blockage ratio case [14] and the mechanism of energy focusing for transition to detonation. They found in these cases that a large turbulent region extended in front of the flame and detonation occurred when shocks collided and created a hot spot, which is consistent with direct initiation. Because of the large turbulent region, they found detonation was more sensitive to initial conditions in this regime. The results of Goodwin et al. [5] indicate that DDT may occur through different mechanisms in different scenarios.

Instead of considering rectangular obstacles along channel walls as many studies have done, Ogawa et al. considered arrays of obstacles [15,16] on a plane. A 2D array of square obstacles in unconfined hydrogen–air was simulated in [15]. Similar to other studies [4,12,13,17], a one-step Arrhenius reaction model was used. In the case of arrays of obstacles, not all directions of flow have the same obstruction configuration. Their results showed that variation in obstruction directions had effects on flow velocity and the strength of pressure waves. More obstructed paths had a slower velocity because of increased momentum losses, but also produced strong pressure waves more quickly and therefore led to the initial DDT in those directions. It was noted that increasing the burning

surface area and turbulence increased the energy addition and accelerated the flow, followed by the formation of shock waves. The study found that the initial detonation resulted when a reflected shock from an obstacle collided with the flame front. Ogawa et al. also considered a 2D array of cylindrical obstacles [16] at several inclinations to the flow. The cylindrical obstacles eliminated the effect of angle of attack present with the square obstacles. Three stages were observed in the acceleration: increased burning surface area accelerated the flow, shock–flame interactions further accelerated the flow once supersonic speeds were reached, and ultimately a steady-state supersonic propagation. The authors noted that turbulence played a big role in the first of these stages. Similar to [10,12], local explosions were observed. However, these explosions did not necessarily result in full detonation of the flow, with the zero degree inclination case not detonating at all in the computed space and time.

As noted, a number of the studies on DDT used a one-step Arrhenius model for modeling chemistry. Some of these studies observed detonation initiation occurring at hot spots ahead of the flame. Ivanov et al. [18], however, suggests that the results are an artifact of the simplified kinetics because the temperatures in front of the flame were actually too low to ignite a detonation given the time scales of the process. Ivanov et al. [18] supported this with a discussion of results from simulations using more detailed chemical reaction models involving multiple steps [19–21] as well as data from experiments [22–24]. Analysis of the results showed that the one-step models allowed ignition at unrealistically low temperatures.

While a few of the numerical studies have been performed in three dimensions, most have been conducted on two-dimensional geometries to keep computational costs reasonable. Valiev et al. [25] considered the differences between planar and axisymmetric simulations. They found that the flame accelerates faster in the axisymmetric case compared to the planar geometry. Similar to findings in [7], the results of Valiev et al. [25] showed that as the flame accelerates, the flame propagation velocity eventually reaches an approximately steady state value.

The goal of this study is to extend the understanding of specific physical mechanisms which contribute to the processes of flame acceleration and transition to detonation by expanding the types of geometries considered. Most of the previous studies on DDT in obstructed flows have focused on rectangular obstacles, but in real world scenarios there are many more potential obstacle types. While studies have considered variations such as blockage ratio and spacing, the influence of the sharp rectangular corners on the ability for a flow to reach DDT has not been considered. From a risk perspective, we would like to know if there are other obstruction shapes which are less likely to promote transition to detonation. The approach taken here is to consider unique obstacle geometries in an effort to isolate what appear to be the most important contributors to DDT caused by obstacles, namely increased mixing and strong pressure wave interactions. We add to previous studies by including detailed chemistry models to better capture the combustion process, and by introducing unique geometries to isolate contributing factors to DDT. In addition to isolating factors associated with DDT, the unique geometries provide insight into how sensitive detonation is to varied obstacle shapes and identify obstacle characteristics which promote DDT. Together, the results of this study improve the understanding of the DDT mechanism and will lead to better risk assessments for scenarios involving uncontained failures that pose a threat to personnel.

2. Approach

The physics of problems considering DDT are quite complex and interactions occurring at very small temporal and spatial scales

can have large effects on the processes of interest. Computational simulation of these flows must be capable of resolving flow instabilities, turbulence, and combustion processes sufficiently to produce correct macroscopic trends without becoming so complex as to be computationally impractical. These constraints have led researchers to simplifications, such as using one-step chemistry models, and developing their own tuned models. In this study, we apply a general use computational tool which includes detailed chemical kinetics.

2.1. Code

The computational fluid dynamics (CFD) code Loci-Chem [26,27] was used for all simulations in this study. This code was originally developed at Mississippi State University and has more recently been further developed in collaboration with NASA. Loci-Chem is a density-based, finite-volume, unstructured solver with second order accuracy in time and space. It is capable of solving the Navier–Stokes equations for three-dimensional, viscous, turbulent, and chemically reacting flows and is therefore a good candidate for modeling the complex flow with finite-rate chemistry problem of interest in this study. The basic governing equations are presented in [Appendix A.1](#).

2.2. Mesh

General mesh parameters were consistent between all geometries considered. We generated unstructured, isotropic grids with an advancing front algorithm [28]. The mesh was refined near the walls. The base shape of all the geometries is a tube, which was assumed axisymmetric. Therefore two-dimensional meshes were generated for half the tube height in a single radial plane.

Gamezo et al. [4] report a laminar flame thickness of 0.35 mm for H₂–air. The results of the geometry sensitivity presented here used a mesh spacing of 125 μm, providing approximately 3 cells per laminar flame thickness. This is within the range of mesh resolution in the literature, though it is somewhat coarser than most. In an effort to determine the degree of mesh sensitivity at this level of refinement, additional meshes for the rectangular obstacles case were generated at cell sizes of 254 μm, 62.5 μm, and 30 μm, or 1.4, 5.6, and 11.7 cells per laminar flame thickness, respectively. The results showed that the initial propagation, when the flame was moving slowly, was sensitive to grid spacing at this level of resolution. This is consistent with [8] which stated that 10 μm was required for mesh convergence based on comparing flame propagation near the ignition point. The behavior of the propagation, once the flame had accelerated on passing the initial obstacle, was observed to be much less sensitive to resolution for the meshes applied here. The detonation location was observed to be somewhat dependent on mesh resolution, but the detonation mechanism appears to be the same for all the meshes applied. The 125 μm resolution was, therefore, judged sufficient to assess the sensitivity of the transition mechanisms to the geometric variations of primary interest here.

2.3. Models

We initialized each simulation with stoichiometric premixed hydrogen–air at 1 atm, 298 K, and zero velocity. Considering a trade-off between complexity of chemical reactions and computational time and resources, we chose a 7-species, 8-reaction model by Evans and Schexnayder [29] as the chemistry model. The species included were H, O, H₂O, OH, O₂, H₂, and N₂. The reaction rates were described by an Arrhenius equation in the form $k = AT^b \exp(-C/T)$ which are given in detail in [29] and [Appendix A.2](#) along with the reactions.

Transport and diffusion models were specified as transportDB, a built-in model in Chem that uses a database of interpolated values for species viscosity, conductivity, and diffusion coefficients [30]. Small scale turbulence was modeled using Mentor's Baseline Model (BSL) which is a combination of $k-\epsilon$ away from the wall and $k-\omega$ near the wall. This model was chosen because it has been found to work well for high speed flows [31].

In addition, we used the Barth flux limiter. This limiter tended to be more stable than other options at high pressures which was needed as the flow accelerated to detonation. While the proposed method and combination of models seemed to work well for this study, further work will be completed in the future to test how sensitive the results are to the chosen models.

2.4. Setup verification and validation

To ensure the CFD code with the chosen models was capable of capturing detonation waves accurately, we computed one-dimensional detonation tests with the same computational setup as used in the remainder of the presented work. The results of the one-dimensional tests were compared with the theoretical Chapman–Jouguet (CJ) condition for detonation waves in stoichiometric H_2 -air at 298 K and 1 atm. The CJ values used for comparison were taken from [31]. Temperature, density, pressure, mass fraction of H_2O , and velocity were considered. Outside of an overpressure spike seen in pressure and density, the computed values compared well to the CJ values. Both temperature and mass fraction of H_2O remained within about 1% and velocity remained within 1.6%. Prior to the spike, pressure deviated by 1–2% and density was closer to 3%. Overall, the close comparison between the CJ values and these results suggest that the chosen CFD code and models are appropriate for capturing detonation wave results.

We also considered the applicability of 2D simulations for this problem. The computational cost of 3D simulations with detailed chemical kinetics on a refined mesh is quite large and limits the number of simulations possible. Two-dimensional, or quasi-2D as is the case here with the axisymmetric assumption, allow for more studies to be computed. While some aspects of the flow are likely to be different without 3D effects, previous studies have shown that 2D simulations are comparable. Both Gamezo et al. [4] and Goodwin et al. [5] computed a 3D case and found that the flame development and DDT mechanisms were the same between the 2D and 3D case suggesting that 2D simulations were sufficient.

The simulations presented in this paper are Reynolds averaged Navier–Stokes (RANS) simulations. Many of the previous studies conducted have used implicit large eddy simulations (ILES). While the grid spacing is refined, it is still relatively coarse in comparison to studies using ILES which typically use grid spacing on the order of 20 μm with some as refined as 3.3 μm . Comparing with the 125 μm grid spacing used in this study, we have a factor of approximately 10–40 larger grid spacing and a factor of approximately 40–1500 fewer cells. As we are at least an order of magnitude coarser than the literature for ILES, we feel it is reasonable to continue with RANS simulations for this study. Future work will include further investigation into whether the RANS model is necessary at this level of mesh refinement.

3. Results and discussion

We are interested in flame propagation in a confined space and the potential for the flame to accelerate and transition from deflagration to detonation. To study this, we considered several geometric variations consisting of the same basic tube, but with different shaped obstacles (Fig. 1). As more results were generated, the geometries were adjusted to provide insight into specific flow phe-

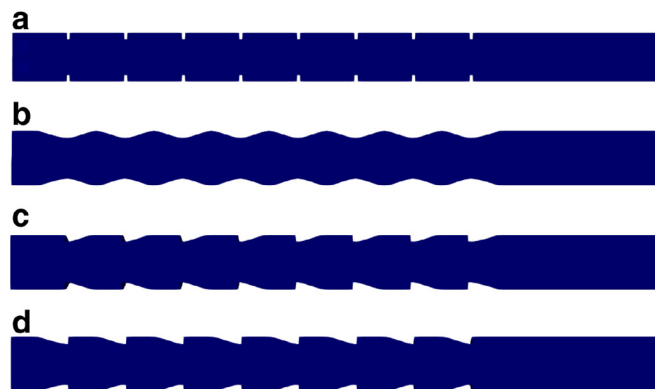


Fig. 1. Geometry of the full tube cross-section with (a) rectangular obstacles, (b) curved obstacles, (c) forward rectangular obstacles and aft curved obstacles, and (d) forward curved obstacles and aft rectangular obstacles. Note only half the tube height is computed in the simulations because of axisymmetric conditions.

nomenon. In the following sections we describe the configurations and present the associated results.

3.1. Configuration 0: no obstacles

An unobstructed geometry was considered initially to establish a baseline result with which to compare other geometry variations. This initial geometry was a simple 60 cm long tube with a 5 cm diameter and no obstacles. The wall boundary condition was an adiabatic no-slip wall, the front and back faces were symmetry planes, the center line was axisymmetric, and the tube ends had reflective boundary conditions. We ignited all geometries by adding energy to the flow at the left end of the tube.

In this configuration, the flow propagated at a relatively constant average speed and did not accelerate significantly or transition to detonation. The flow was interesting in that it developed a distorted tulip flame, similar to what has been noted by other studies for unobstructed channels and pipes [32–35]. The tulip flame is characterized by the flame propagating faster at the tube walls and developing a cusp at the center line. It transitions to a distorted tulip flame, characterized by additional tulip petals developing on the original tulip. While the flame propagation for this case was interesting, it gave us little insight into DDT mechanisms on its own since the flow did not detonate within the given tube length. The comparisons of other geometries to this case will be the source of further DDT understanding.

3.2. Configuration 1: rectangular obstacles

In this configuration, we added obstacles to the flow in order to induce DDT. We investigated how the addition of these obstacles changed the flow in comparison to the baseline case. This geometry was chosen because there is available experimental and numerical data matching these [9,31], or similar [8,11], dimensions with rectangular obstacles. We chose eight, evenly spaced, rectangular obstacles with a blockage ratio of 0.43 for the first obstructed geometry, shown in Fig. 1(a). Blockage ratio was calculated as the ratio of the area blocked by the obstacles to the cross sectional area of the tube. As in the baseline case, the length of the tube was 60 cm and the diameter was 5 cm. The obstacles were placed one tube diameter apart. The boundary conditions were the same as the baseline case, with the addition of adiabatic no-slip walls on the obstacles. The simulation was computed with a time step of $1e-7$ s until detonation occurred. The time step was chosen for numerical stability.

A time sequence of temperature contours from ignition through detonation for this case is presented in Fig. 2(a). The first frame

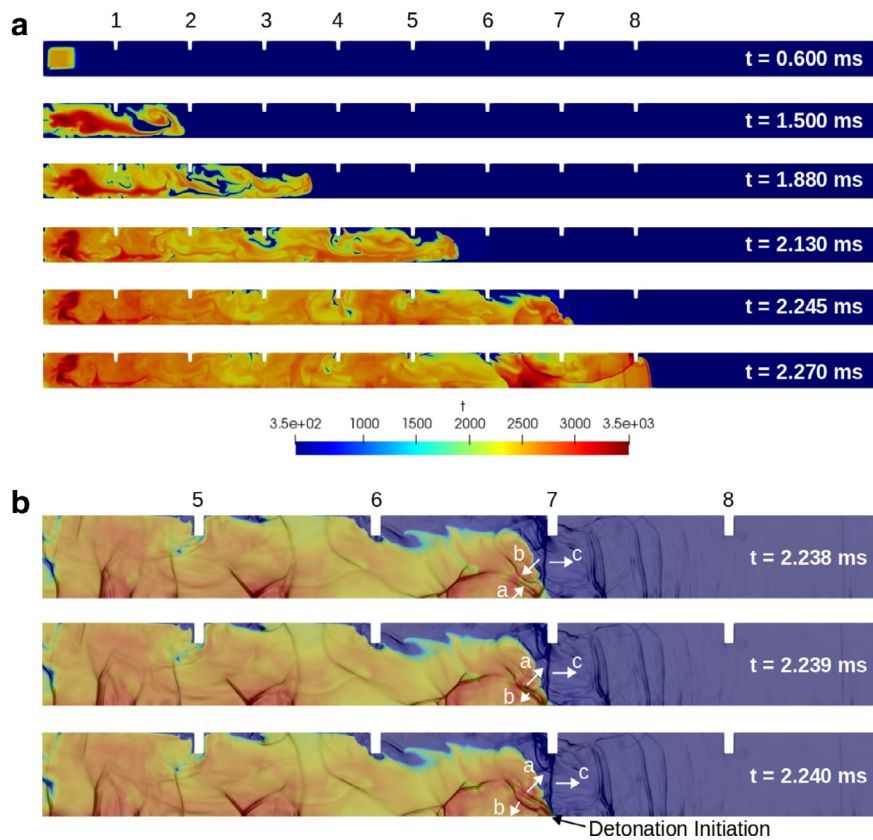


Fig. 2. (a) Sequence of temperature contours to show flame propagation from ignition through detonation for the tube with rectangular obstacles. Detonation is seen in the fifth frame. Time between figures is not constant. (b) Temperature contours with pressure gradient overlay at point of detonation showing strong pressure waves colliding at flame front. Arrows show direction of the pressure waves. Obstacles five through eight are shown.

shows where ignition began on the left end of the tube. Once ignition occurred and as the flame propagated, flow was induced ahead of the flame due to the expansion of burned products. Vortical flow features developed behind the obstacles in the flow ahead of the flame as well as pressure waves which propagated through the tube. Initially the flame propagated slowly, and as the flame interacted with the first obstacle, the flow accelerated because of reduced area (obstacle blockage). The flow over the first obstacle is observed to separate and cause the formation of an annular vortex between the first two obstacles, increasing the burning surface area and entraining unburned fuel within the flame region as shown in the second frame. The flame continued to propagate and accelerate as it interacted with more obstacles in frames three and four, expanding after each obstacle and trapping and burning fuel in the space between obstacles, leaving the flow well mixed. Eventually, the flow detonated on the flame front along the center line at obstacle seven, shown in frame 5. The detonation looks similar to results for other rectangular obstacle studies [8,31] where the detonation also occurred near the center line at the flame front. Other studies [4,13], however, have found that the detonation initiates in the corner of an obstacle after a Mach stem interacted with the obstacle to create a hotspot. In the present simulation, following the onset, the detonation grew radially, reflecting off the wall and passing the last obstacle. The last frame shows the nearly fully developed detonation propagating past the last obstacle. The flame front continued propagating essentially as a plane wave to the end of the tube. This sequence of ignition, slow flame, deflagration, acceleration, and detonation is similar to what previous studies have shown.

Analysis of the results indicate that, in addition to the flow accelerating, the development and reflection of strong pressure waves were a key factor in the transition to detonation. These

results support the conclusion of previous studies regarding the importance of shock interactions in the DDT process. For example, Khokhlov and Oran [36] stated that their main conclusion from the study was that shock and flame interactions were important to create conditions that allowed DDT. In order to better analyze the pressure wave and flame interactions, pressure gradients are overlaid on temperature contours in Fig. 2(b). These images provided visualization of the pressure waves interacting with the geometry, the flame, and other pressure waves. A strong pressure wave reflected off the wall between obstacles six and seven and traveled towards the center line. The wave then reflected at the center line because of the imposed symmetry which required a matching pressure wave to be coming from the other wall. The original reflection (labeled c) continued on the right of the flame front and interacted with obstacle 7 forming the normal shock. The second reflection formed the curved pressure wave (a) to the left of the flame front. As these two interacting waves propagated through the flame and met the flame front, along with another reflected pressure wave (b) off of obstacle 7, a high pressure spot formed on the center line at obstacle seven where the pressure waves interacted, and detonation was initiated. As the detonation expanded and propagated, the flame overtook the pressure waves observed in front of the initiation point in Fig. 2(b). Once the detonation was fully developed in the tube, the leading pressure wave coincided with the flame front. Note that there were also strong pressure waves interacting behind the flame front, which do not initiate detonation of the flow because of the lack of sufficient unburned fuel. The detonation was only able to propagate when there was unburned fuel available.

The pressure waves in the flow originate when the hot regions of expanding combustion products cause rapid expansion of unburned gas. The flame acts somewhat like an accelerating piston,

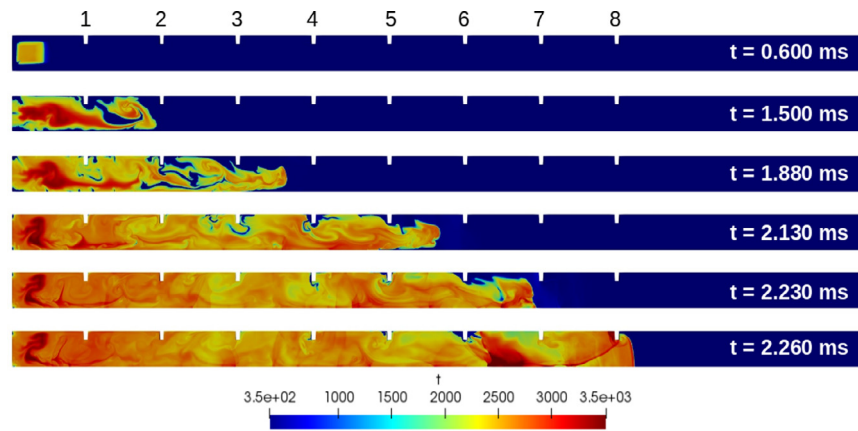


Fig. 3. Sequence of temperature contours to show flame propagation from ignition through detonation for the tube with rectangular obstacles and non-reflective boundary condition. Detonation is seen in the fifth frame.

producing compression waves that then reflect from the wall and obstructions. In general, the reflection of these waves from walls and obstacles, and the interaction of these waves, tends to amplify them, ultimately creating a high-pressure zone sufficient to initiate detonation. There was some concern that since detonation occurred on the center line, the pressures may have been artificially high there because of the axisymmetric boundary condition. The axisymmetric condition forces pressure waves reflected from the walls around the entire tube to be symmetric and meet exactly at the center line. In three dimensional situations, it is unlikely that pressure waves would come together so exactly because of small perturbations in the flow. This would reduce the high pressure region at the point of detonation initiation. More on this will be discussed for other configurations.

3.2.1. Further development

Before considering other geometries, additional sensitivities were performed with this geometry to ensure the robustness of the results. The first parameter considered was the wall (and obstacle) boundary condition. Both slip and non-slip conditions at the wall and on the obstacles were simulated. The bulk flow was viscous for all cases; only the wall boundary conditions were varied. The results showed that the case with no-slip walls detonated one obstacle sooner than the slip walls case. The mesh generated for the case with no-slip walls had refined, structured cells along the boundary and the case with slip walls did not. To ensure the differences were not a result of the mesh, an additional case was computed in which the slip wall condition was applied, but with the mesh generated for the no-slip wall condition. The detonation initiation in this case also occurred later than in the no-slip case, suggesting the effect was, in fact, an effect of the boundary condition and not the mesh. Some of the differences could also be due to model uncertainties outside of the mesh. Additionally, a computation with reduced time step produced a similar detonation initiation. The flow in the case with slip walls also propagated faster, likely because the flow in the no-slip case was losing energy to friction at the walls. A trend observed in the cases computed here is that changes that generally slow the flow shorten the physical distance to detonation. This assumes the flow still has significant acceleration and is not just propagating consistently like the unobstructed case. While the physical location changed with the boundary conditions, the time to detonation remained about the same.

In addition to the wall boundary condition, the boundary condition on the right end was considered for the rectangular obstacles case. Most of the simulations presented use a reflective boundary condition. A non-reflective boundary condition was also

simulated for this case. The results showed little difference between the propagation. Temperature contours for the case with a non-reflective boundary condition on the right end of the domain are shown in Fig. 3. Comparing with Fig. 2(a), the first four frames are essentially identical. Note in frame five that the detonation occurs slightly earlier in time and space for the case with the non-reflective boundary condition. However, once detonation occurs, it continues to propagate very similarly to the previous case. Based on these results, the boundary condition at the right end seems to have little effect on the transition from deflagration to detonation for this geometry.

The ignition source location, size, and intensity were also varied. The position of the ignition source was on the left end and moved vertically from the center of the half channel (as shown in Fig. 2(a)) to the center line. The size of the ignition source was adjusted so the same amount of energy, for constant heat flux, was added in both cases. Shifting the ignition source to the center line made little difference in the propagation, acceleration, and eventual detonation of the flow. The size and intensity of the ignition source, however, affected the ignition and initial flame propagation process. Reducing the overall energy input (same energy flux with smaller initial ignition area or larger energy flux with significantly smaller initial ignition area) produced slower initial flame speeds such that the flame took longer to reach the first obstacle. Once the flame reached the first obstacle, the propagation remained very similar for all ignition source variations. Detonation also occurred in approximately the same locations. While the ignition source did affect the overall time to detonation because of the effect on the initial flame propagation, the propagation through the obstacles and the likelihood of detonation was not significantly affected, as long as enough energy was supplied to ignite the flow.

Results of the simulation variations show that the results were not overly sensitive to things like ignition source placement and mesh refinement at the walls. With confidence in the approach, we now turn to geometry variants to gain additional insight into the DDT process.

3.3. Configuration 1.5: no obstacle 7

From the case with evenly spaced rectangular obstacles, we saw pressure waves reflecting at obstacles and have shown the interactions of the reflecting waves to be important for detonation. Other studies have also commented on the importance of pressure waves interacting with the obstacles. For example, [4] said that reflection of strong shocks generated by the accelerating flow were

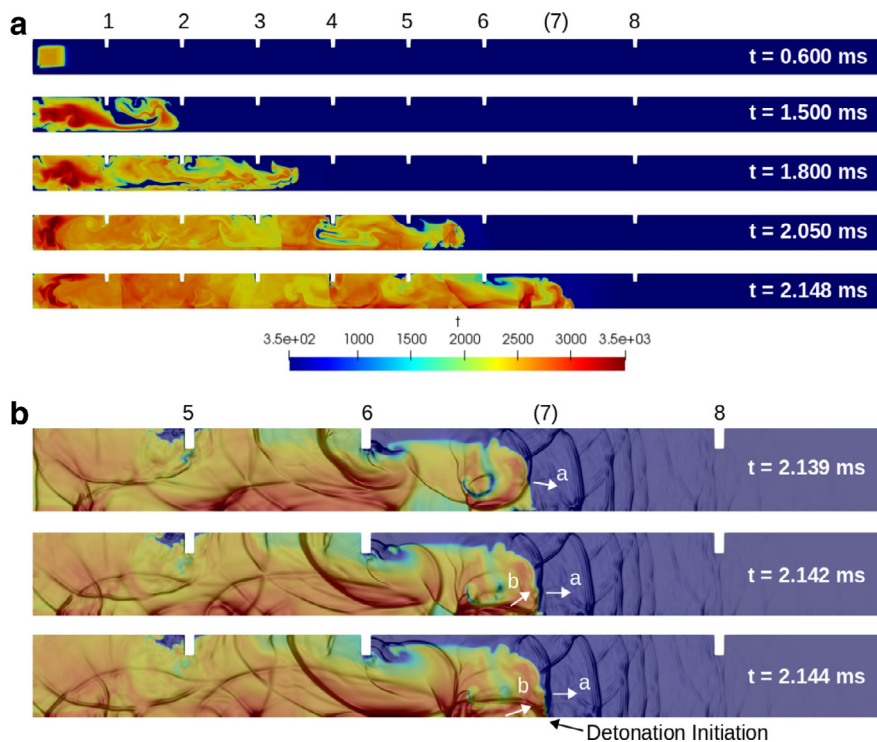


Fig. 4. (a) Sequence of temperature contours to show flame propagation from ignition through detonation for the tube with the seventh rectangular obstacle removed. Detonation is seen in the fifth frame. (b) Temperature contours with pressure gradient overlay at point of detonation showing strong pressure waves colliding at flame front. Arrows show direction of the pressure waves. Obstacles five, six, and eight are shown.

needed to create hot spots that potentially allow for detonation. In an effort to investigate the sensitivity of specific obstacle placement, we eliminated the seventh obstacle, where the detonation occurred in the previous case. The geometry is shown in Fig. 4(a). All other boundary and initial conditions remained the same as in Section 3.2.

Temperature contours for the case without obstacle seven are presented in Fig. 4(a). The first frame shows the location of the ignition source, followed by additional frames showing the flame propagation. The flow is visually similar to the first case. The last frame in Fig. 4(a) shows the start of detonation at the flame front along the center line and at the location where obstacle seven was previously. Eliminating the obstacle at the point of detonation, and the potential for pressure wave reflections off that obstacle, did not change the overall results.

There were still sufficient pressure wave interactions to allow for detonation even without the obstacle, presented in Fig. 4(b). Pressure waves traveled from the top wall towards the center line where the wave reflected. The original pressure wave (labeled a), plus the reflected wave (b) off the center line, interacted at the flame front and allowed for a point of detonation as depicted in the final frame of Fig. 4(b). This path of pressure reflections was the same as the case with all eight obstacles. The main difference in the pressure waves at the point of detonation was that the top part of the pressure waves near the wall (where the obstacle was removed) did not coalesce. This had little effect on the detonation since the critical interaction occurred on the center line. Outside of looking at the pressure wave interactions for DDT initiation, the pressure waves ahead of the flame are interesting and shown clearly in this case. They appear distinct, and may be generated by discrete flame accelerations. Rather than the flame gradually accelerating, these pressure waves suggest the flame increases speed in bursts which generate pressure waves through a piston-like effect. These waves were also seen in the previous case and will be discussed further in Section 3.7.

We can conclude from these results that the point of detonation is relatively insensitive to exact obstacle placement and the reflections off any specific obstacle are not critical to detonation. While pressure wave interactions still appear to be an important factor in the DDT process, the results may suggest that the reflections and interactions push the flow over the edge as opposed to driving the transition to detonation. It could be that the flame has accelerated to a point that it is primed for detonation and looking for a pressure jump somewhere to help it transition and the pressure wave interactions from the reflecting waves provide that. Further study will include eliminating more obstacles to observe how early the conditions for detonation are actually set up.

3.4. Configuration 2: curved obstacles

The next geometry we considered featured larger changes to the obstacles. In this geometry, we investigated the effect of removing all corner reflections, while keeping the blockage ratio the same. The geometry, shown in Fig. 1(b), eliminated the forward corner reflections and reduced the aft separation zone by rounding the obstacles. The peaks of the rounded obstacles remained one diameter apart with a blockage ratio of 0.43 (peaks of the rounded obstacles were the same height as the rectangular obstacles). Keeping the blockage ratio the same ensured that acceleration caused by flow constriction between the cases remained constant. We could then focus on flow characteristic changes resulting only from forward and aft obstacle shape changes. The boundary conditions also remained the same as previous cases.

In this case, the flow did not detonate within the length of the tube and the flame propagation was qualitatively different from the rectangular obstacles case. Rather than distorting and leaving unburned pockets of fuel as in the rectangular obstacle case, the flame here followed the obstacles closely and smoothly propagated along the wall, leaving very little unburned fuel behind the flame front. The elimination of the bluff body on the forward side of the

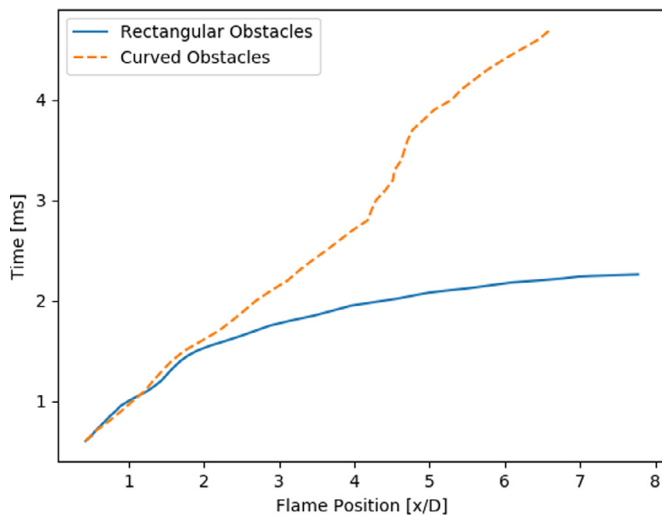


Fig. 5. Plot of time vs location for the rectangular obstacles and curved obstacles cases showing acceleration for the rectangular obstacles case and little acceleration for the curved obstacles case.

obstacle allowed the flame to more smoothly decrease in area to pass through the obstacles. The bluff body previously forced the flame to separate from the wall prior to reaching an obstacle. Also, the elimination of the aft bluff body reduced the separation and recirculation zone behind the obstacles, again allowing the flame to propagate more smoothly and follow the curve of the wall.

To compare the flame propagation, Fig. 5 shows flame position versus time. Flame position was defined as the forward-most point of the flame. The plot shows a clear difference in the acceleration behavior in the two cases. The data representing the flow for the rectangular obstacles shows that the flame front accelerated quickly in the first few obstacles, while the data for the curved obstacles flow has a relatively constant slope indicating very little flame acceleration and a more constant and slower flame propagation speed. The jump in the plot after the fourth obstacle for the curved obstacle case is a result of the interaction of the flame with pressure waves that have been reflected from the right end of the tube. The results for the curved obstacles case are more similar to the unobstructed flow originally considered than to the rectangular obstacles case. Neither the unobstructed flow or the curved obstacles flow accelerated significantly or detonated. While the shape of the propagating flame was different between the two cases, the propagation speeds were comparable. Other studies [32,33] looking at unobstructed flows have also shown results for position versus time that are similar to the curved obstacle case results with regions of constant velocity between small jumps in velocity.

The curved obstacles, while obstructing the flow, in general did not provide the same sustained flame acceleration required for detonation. Therefore, simple area reduction was not the driving cause of flame acceleration in the rectangular obstacles case. Other factors that could result in acceleration of the flow are increasing the burning surface area and increasing the vortical structures in the flow. A comparison of the burning surface area is presented in Fig. 6(a). Burning surface area was computed by creating an iso-contour of the flame surface in the computational domain (based on temperature), revolving the contour about the center axis of the tube, and calculating the total surface area, including the area surrounding unburned pockets of fuel. As the flame propagated in the rectangular obstacles case, the burning surface area increased and then leveled out until detonation where the surface area decreased. The curved obstacle case, however, showed a small increase in burning surface area initially, but then remained low in

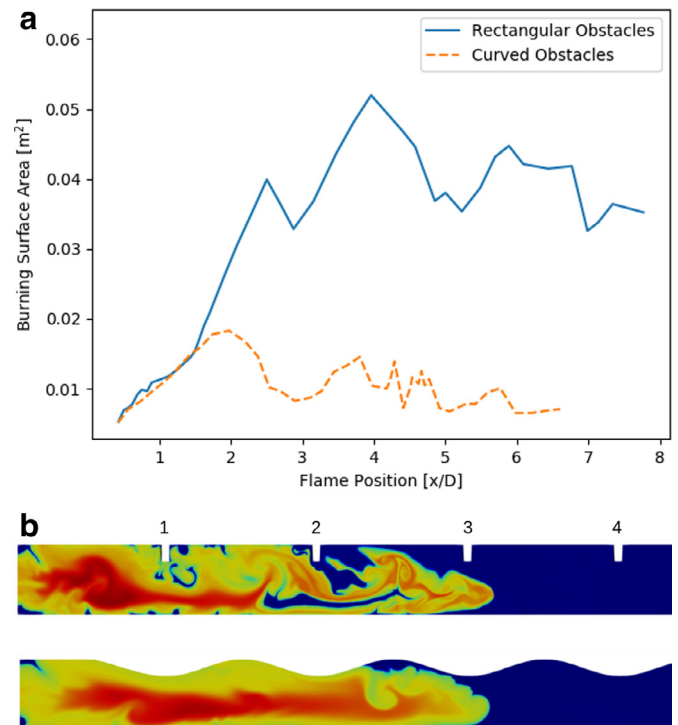


Fig. 6. (a) Plot of burning surface area vs location for the rectangular obstacles and curved obstacles cases showing an increase for the rectangular obstacles case and little increase for the curved obstacles case. (b) Temperature contours for the rectangular obstacles case and the curved obstacles case showing the difference in burning surface area. Obstacles one through four are shown.

comparison to the rectangular obstacles case. The trends in the burn area (Fig. 6(a)) and acceleration (Fig. 5) results provide support for the conclusion that the flame distortions and associated increase in burn surface area in obstructed flows are a primary contributor to the flame acceleration, also a stated conclusion in [4,12,16].

Figure 6(b) presents temperature contours at similar locations along the tube for the rectangular obstacles case and the curved obstacles case. Again, it is clear that the burning surface area of the curved obstacles case was significantly lower. The flame in the curved case followed the walls closely, limiting the burning surface area, whereas the flame in the rectangular case was more complex with regions of unburned material trapped behind the flame front, increasing the burning surface area. The results of this geometry in comparison with the previous geometries demonstrate that one of the roles of the obstacles in reducing the time to detonation is to quickly accelerate the flow by breaking up the flame and increasing burning surface area. This was especially important as the flame passed through the first few obstacles where we saw the big differences start to form between the obstructed and unobstructed cases. Some obstructions are better suited than others to encourage this more complex flow, which will be investigated further.

3.5. Configuration 3: aft curved obstacles

Results of the previous sections indicate the presence of obstacles produces flow features ahead of and behind the propagating flame that appear to be responsible for flame acceleration and, ultimately, transition to detonation. It is, however, unclear what specific flow features that are created by the obstacles are more responsible for this flame acceleration. The rectangular obstacles provided these conditions while the curved obstacles did not. We would like to look at geometries that may help to isolate the

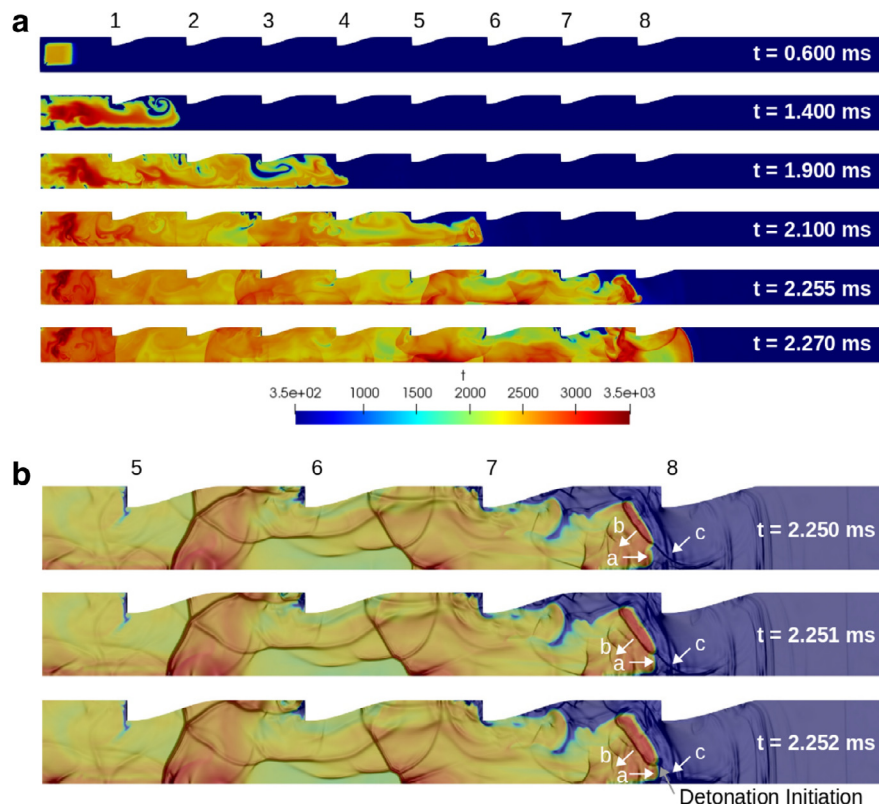


Fig. 7. (a) Sequence of temperature contours to show flame propagation from ignition through detonation for the tube with forward rectangular obstacles and aft curved obstacles. Detonation is seen in the fifth frame. (b) Temperature contours with pressure gradient overlay at point of detonation showing strong pressure waves colliding at flame front. Arrows show direction of the pressure waves. Obstacles five through eight are shown.

features that appear to be most responsible for the initiation of detonation in these cases. The next geometry, depicted in Fig. 1(c), was a combination of the rectangular and curved obstacles. The forward part replicated the rectangular while the aft part replicated the curved obstacle. We used the same spacing, blockage ratio, and boundary conditions as the previous cases. The goal for this geometry was to maintain surfaces for reflecting pressure waves back to the flame while reducing the vortex shedding and mixing from the aft surface.

A sequence of temperature contours showing the flame propagation for this case is presented in Fig. 7(a). In general, the flame looked more similar to the rectangular obstacles than the curved obstacles case. The flow ignited in the first frame of Fig. 7(a) and then accelerated as it moved through the next several frames. Despite removing the aft bluff body, the temperature contours show that there was still visible vortical mixing of the flow for this geometry, likely because the flow still separated as it came off the forward bluff body. As a result, we still see similar characteristics to the rectangular obstacle case like the flame curling back on itself and trapping some unburned fuel. In the fifth frame, detonation has been initiated at the flame front, away from the center line. The detonation continued into the last frame where the flame reflected off the wall and spread across the diameter of the tube. Here, the detonation occurred at obstacle eight, whereas the rectangular obstacle case detonated at obstacle seven. The fact that the detonation did not initiate directly on the center line for this case argues that the detonation initiation is not purely an artifact of the axisymmetric boundary conditions. While the axisymmetric condition may have had an effect in previous cases, the overall mechanism of converging strong pressure waves creating conditions that allow for detonation shown previously is supported by these results.

As expected with this geometry, the pressure waves did stack and reflect off the forward part of the obstacles. Figure 7(b) presents temperature contours with overlaid pressure gradients at the point of detonation. The same mechanism of strong pressure waves coming together in unburned fuel seen in the rectangular obstacles cases was observed here. In this case, one pressure wave was reflected off of the next obstacle (8) and traveled back towards the flame front and through the flame (labeled b and c). Another pressure wave was generated (a) near the center line as the flame front expanded. The two pressure waves came together at the flame front and detonation initiated in line with obstacle eight and between the center line and the obstacle. Compared to other cases, the detonation location did shift slightly, but the detonation mechanisms are relatively insensitive to exact obstacle placement and shape as long as the obstacles can accelerate the flow.

3.6. Configuration 4: forward curved obstacles

To isolate the effects of mixing from forward facing wave reflections, we reversed the obstacles in this geometry, shown in Fig. 1(d). In this case, the forward part of the obstacle was curved and the aft side was rectangular. This geometry allowed for bluff body separation to increase mixing behind each obstacle, but without the forward corner reflections for pressure waves. The obstacle spacing, blockage ratio, and boundary conditions were the same as the previous cases.

Temperature contours tracking the flame propagation for this case are illustrated in Fig. 8(a). Similar to the other cases with rectangular obstacle variants, the flow was ignited on the left and then began to accelerate as the flame propagated and interacted with the obstacles. The flame was influenced by mixing in the flow, characterized by the convoluted flame and unburned fuel behind

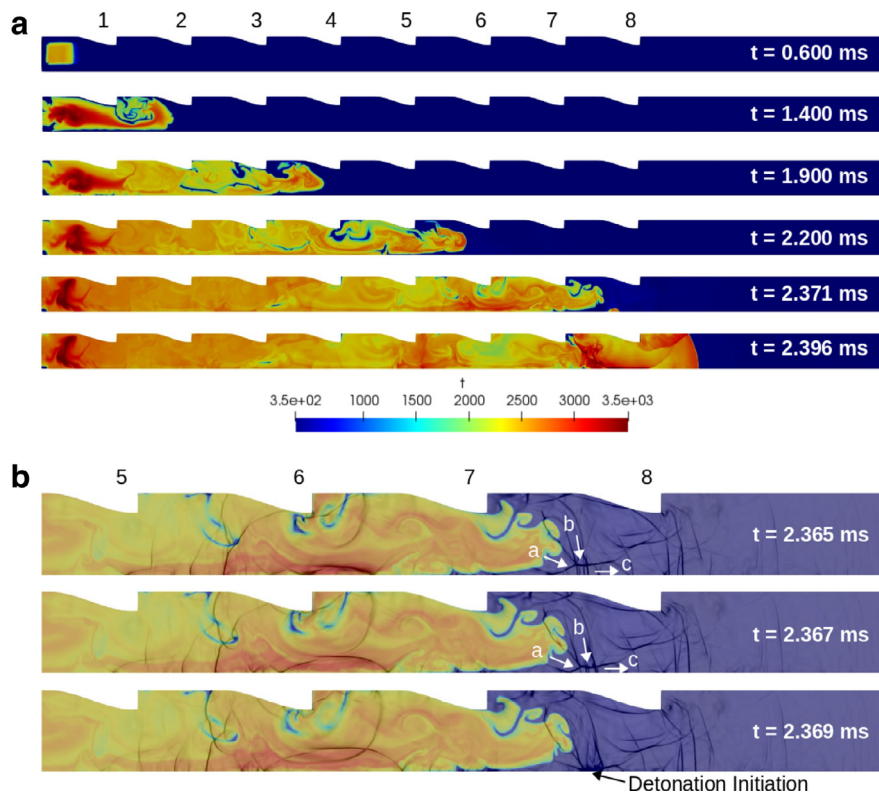


Fig. 8. (a) Sequence of temperature contours to show flame propagation from ignition through detonation for the tube with forward curved obstacles and aft rectangular obstacles. Detonation is seen in the fifth frame. (b) Temperature contours with pressure gradient overlay at point of detonation showing strong pressure waves colliding at flame front. Arrows show direction of the pressure waves. Obstacles five through eight are shown.

the flame front. This was again consistent with the flames seen in the rectangular obstacles case and the forward rectangular obstacle variant. The fifth frame in Fig. 8(a) shows the flame profile shortly after detonation initiation. Detonation initiated at approximately obstacle 7.5, not in line with the peak of an obstacle and between the initiation location observed in the rectangular obstacles case and the forward step case. The detonation initiated approximately where the curved part of obstacle eight began. Detonation occurred on the center line, as has been observed in most of the detonating cases. What is unusual in this case is that the detonation occurred ahead of the main flame front and not in line with an obstacle peak. Previous studies [4] have seen detonation ahead of the flame, but in the corner ahead of the obstacle as opposed to on the center line.

Regardless of where the detonation occurred, it seems to have occurred by the same mechanism in which strong pressure waves coalesce to initiate detonation. Figure 8(b) shows pressure waves converging ahead of the flame at the point of detonation. One pressure wave (labeled b) reflected off the wall and curved part of obstacle eight and traveled towards the center line. Additional pressure waves (a and c) propagated downstream, ahead of the flame, and interacted with the reflected waves, allowing for detonation. While the axisymmetric condition may have played a factor in the location of the detonation initiation, it is also likely that the current geometry encouraged the pressure waves to reflect in a way that focused them ahead of the flame. In Fig. 8(b), the pressure waves appear to be angled away from the flame. It is interesting to note that strong pressure waves and reflections were still able to form with this geometry despite removing the forward corner reflections by curving the forward part of the obstacle, suggesting that reflections off the forward part of bluff body obstacles is not necessary for transition to detonation to occur. This agrees with the results of the rectangular obstacles case with

obstacle seven removed where the reflections off the obstacle were not needed for detonation.

3.7. Comparisons

Both of the mixed rectangular and curved obstacles cases behaved more similarly to the rectangular obstacles case than the curved obstacles case in that both accelerated and eventually detonated. A comparison of the flame location propagation is shown in Fig. 9(a). The propagation is very similar among the three cases with some form of rectangular obstacles. The small differences in acceleration can be attributed to geometry and modeling uncertainty. These results provide support for the conclusion that the obstacles act to increase the flame area, resulting in an accelerated flame, which creates conditions favorable for detonation. The specific obstacles may not matter as much.

Flame front velocity is presented in Fig. 9(b). The case without sharp obstacles is, again, qualitatively different from the other cases. This plot does reveal subtle differences between the cases with sharp edged obstacles and also indicates the presence of oscillations superimposed on the general trend of increasing flame speed. The oscillations correlate with the peaks and valleys of the obstacles and are a potential source of pressure wave generation. Note that the rectangular obstacles seem to produce the strongest of these velocity oscillations. The large spikes in velocity denote when detonation was initiated.

Because the propagation and acceleration were roughly similar for the three rectangular obstacles variations, we expect that the burning surface area and vortical features are also similar since they are contributing factors to acceleration. Burning surface area for all the cases is presented in Fig. 9(c) and does show that the two mixed cases were more similar to the rectangular obstacles case. The burning surface area for the two mixed obstacles cases

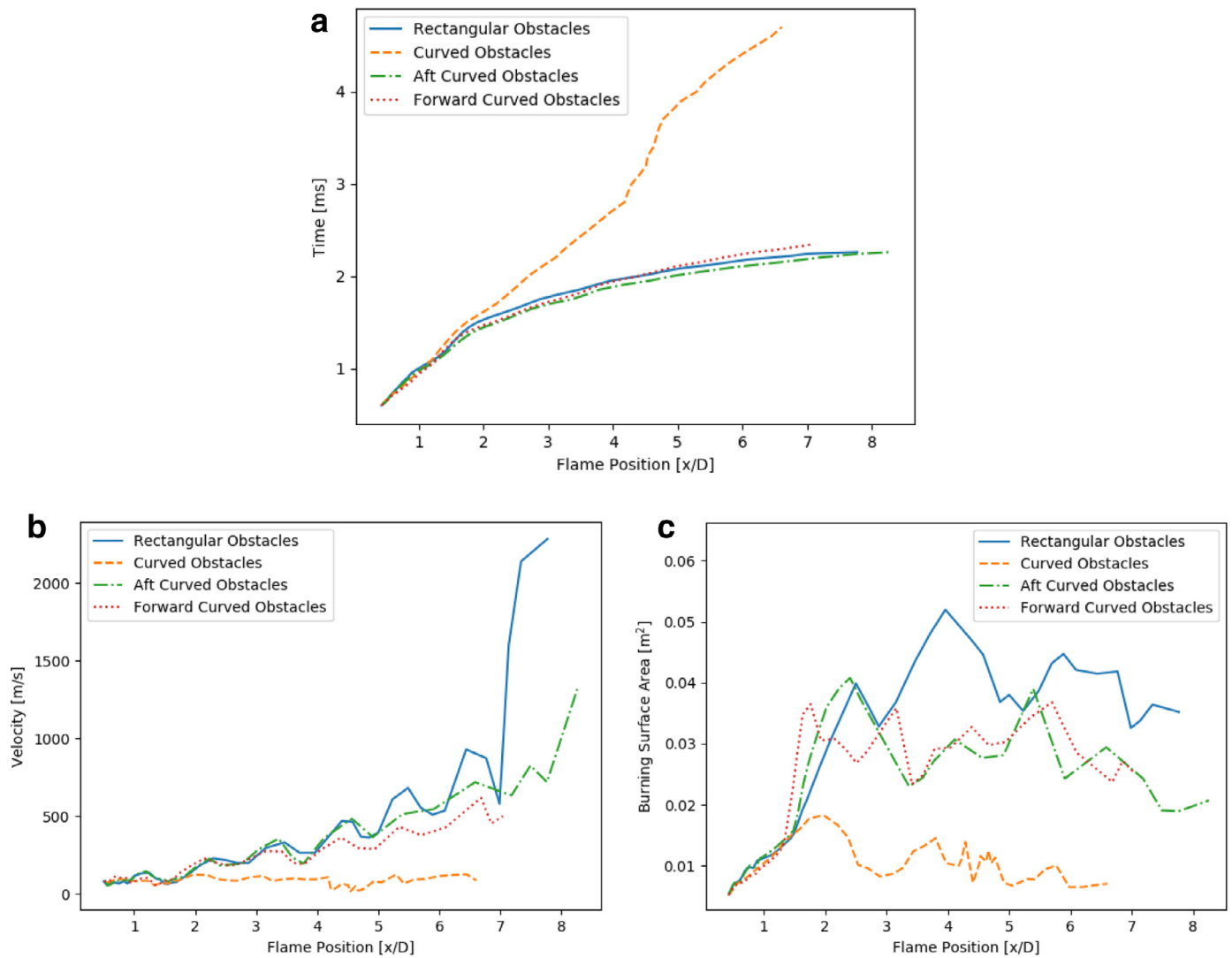


Fig. 9. (a) Plot of time vs location for all cases showing acceleration for the rectangular, forward rectangular, and aft rectangular obstacles cases and little acceleration for the curved obstacles case. (b) Plot of inertial flame velocity vs location for all cases showing increasing velocity for the rectangular, forward rectangular, and aft rectangular obstacles cases and approximately constant average velocity for the curved obstacles case. (c) Plot of burning surface area vs location for all cases showing an increase for the rectangular, forward rectangular, and aft rectangular obstacles cases and little increase for the curved obstacles case.

were qualitatively similar in amplitude. This suggests that the history of energy addition was similar for the two cases and differences in detonation location could be attributed to differences in geometry, specifically, differences in the ability to produce the coalescence of strong pressure waves.

All the cases initially produced increasing flame surface area, but the curved obstacles case showed significantly less flame area increase than the others. In general, the plots suggest that most of the increase in burning surface area was early in the propagation when the flow interacted with the first few obstacles. The flame distortions associated with the initial large increase in burn area led to the sharp initial flame acceleration observed in the propagation data. After the first large flame acceleration, the flame area variations appear to help ratchet up the flame velocity.

Comparing the different cases, there are clear distinctions between the cases with smooth walls and the cases with sharp-edged walls. The temperature contour plots show that there are vortical features in the flow when the geometry has edges that are not observed in cases where there are smooth walls. The geometric edges introduce vortex shedding, contributing to the significant flame distortion observed, which accelerates the flame. The acceleration of the flame produces shock waves ahead of the lead flame,

and during the process of delayed burning in the vortical structures, through a piston-flow-like effect. Differences in the specific geometry within the sharp-edged configurations appears to have some effect on the vortex shedding location and strength, as well as the reflection of generated shocks. These differences appear subtle in comparison to the cases without vortex shedding (smooth walls), but may still offer clues into the specific mechanisms of flame acceleration.

4. Conclusions and future work

In this study we have considered the mechanisms for transition from deflagration to detonation in stoichiometric hydrogen-air mixtures for several axisymmetric geometries including an unobstructed tube and tubes with a combination of rectangular and curved obstacles. We analyzed burning surface area and vortex shedding as methods of flow acceleration, and tracked strong pressure waves to determine their interactions with the obstacles and their role in detonation initiation. Unique geometries were chosen in an effort to isolate individual aspects of the flow.

For the tubes with obstacles cases presented in this study, we observed two main flow conditions in all instances of transition

from deflagration to detonation. First, there was near-field confinement that resulted in reflections of strong pressure waves and those waves interacted in unburned fuel. Pressure wave interactions occurred behind the flame in burned fuel in some cases, and created high pressure regions, but did not become detonations. Only interactions in unburned fuel ahead of, or at the front of the flame, resulted in detonation initiation. These initiations occurred at the point of the strong pressure wave interaction. Cases without strong pressure wave interactions were not observed to detonate.

The second condition observed in cases of DDT was the flow required sufficient energy addition resulting in acceleration. While the flame accelerated just by passing through obstacles, area constriction was not sufficient to accelerate the flow to detonation. We observed the need for the obstacles to create vortical structures in the flow, resulting in increased burning surface area which increased the rate of energy addition. Flows without the complex flow created by vortex shedding were not shown to accelerate and DDT was not observed in the length of the tube domain computed. It should be noted that, while we observed significant vortical structures in many of the cases, the simulations were computed in quasi-2D which eliminated potential 3D effects such as vortex stretching. This could break down some of the well-defined vortical features in the flow we observed as contributing to the needed energy addition and resulting flame acceleration, however, we feel that the important aspect of the vortical features introduced by the presence of obstacles was the distortion of the flame front which is still likely to occur in 3D, even if the coherent vortices are less distinct.

By varying the geometry, we found that geometric effects altered the specifics of pressure wave interactions and acceleration, but did not eliminate either one for the cases with sharp-edged geometries. For these cases, we saw that transition from deflagration to detonation was not overly sensitive to a specific geometry as long as the strong pressure wave interactions and flame acceleration were observed. Additional work is needed to further explore the relative importance of these two features, and whether there are other features not yet identified that may be important.

The results of this study identified further areas of interest to study which will be continued in future work. These include the effect of delayed burning of the eddy-entrained mixture and turbulence modeling. It is difficult to talk about turbulence in 2D and some further thought needs to be done in that area, including looking at the effect of using different turbulence models. A different model may affect features in the recirculation zones behind the obstacles and, consequently, the burning of the entrained mixture. In addition, the difference in acceleration mechanisms between the larger scale eddies and the smaller scale turbulence and associated diffusion is of interest. Because we are ultimately considering flame propagation and acceleration from a risk point of view for rocket engine bays, we will also consider a sensitivity study to background pressures since an uncontained failure could happen at pressures other than atmospheric.

Acknowledgments

Supercomputing resources supporting this work were provided by the NASA High-End Computing (HEC) Program through the NASA Advanced Supercomputing (NAS) Division at Ames Research Center.

Appendix A. Equations

A.1. Governing equations

A detailed explanation of the governing equations solved by the Loci-Chem CFD solver is found in [30], and a summary of the basic

equations for axisymmetric flows are presented here. The governing equations in cylindrical coordinates (z, r, θ) are given by the following equations.

$$\frac{\partial Q}{\partial t} + \frac{\partial E}{\partial z} + \frac{1}{r} \frac{\partial(rF)}{\partial r} + \frac{1}{r} \frac{\partial G}{\partial \theta} + H = \frac{\partial E_v}{\partial z} + \frac{1}{r} \frac{\partial(rF_v)}{\partial r} + \frac{1}{r} \frac{\partial G_v}{\partial \theta} + H_v \quad (1)$$

Here, Q is the vector of conservative state variables, E , F , and G are inviscid fluxes, E_v , F_v , and G_v are viscous fluxes, and H and H_v are coordinate transformation source terms.

$$Q = \begin{bmatrix} \rho \\ \rho u_z \\ \rho u_r \\ \rho u_\theta \\ \rho e_0 \end{bmatrix} \quad (2)$$

$$E = \begin{bmatrix} \rho u_z \\ \rho u_z^2 + p \\ \rho u_z u_r \\ \rho u_z u_\theta \\ (\rho e_0 + p)u_z \end{bmatrix}, \quad F = \begin{bmatrix} \rho u_r \\ \rho u_r u_z \\ \rho u_r^2 + p \\ \rho u_r u_\theta \\ (\rho e_0 + p)u_r \end{bmatrix}, \quad G = \begin{bmatrix} \rho u_\theta \\ \rho u_z u_\theta \\ \rho u_r u_\theta \\ \rho u_\theta^2 + p \\ (\rho e_0 + p)u_\theta \end{bmatrix} \quad (3)$$

$$E_v = \begin{bmatrix} 0 \\ \tau_{zz} \\ \tau_{zr} \\ \tau_{z\theta} \\ u_z \tau_{zz} + u_r \tau_{zr} + u_\theta \tau_{z\theta} - q_z \end{bmatrix}, \quad F_v = \begin{bmatrix} 0 \\ \tau_{rz} \\ \tau_{rr} \\ \tau_{r\theta} \\ u_z \tau_{rz} + u_r \tau_{rr} + u_\theta \tau_{r\theta} - q_r \end{bmatrix}, \quad (4)$$

$$G_v = \begin{bmatrix} 0 \\ \tau_{\theta z} \\ \tau_{\theta r} \\ \tau_{\theta\theta} \\ u_z \tau_{\theta z} + u_r \tau_{\theta r} + u_\theta \tau_{\theta\theta} - q_\theta \end{bmatrix}, \quad H = -\frac{1}{r} \begin{bmatrix} 0 \\ 0 \\ p + \rho u_\theta^2 \\ 0 \\ 0 \end{bmatrix}, \quad H_v = \frac{1}{r} \begin{bmatrix} 0 \\ 0 \\ -\tau_{\theta\theta} \\ \tau_{r\theta} \\ 0 \end{bmatrix} \quad (5)$$

Shear stress components are defined as follows.

$$\begin{aligned} \tau_{zz} &= 2\mu_T \frac{\partial u_z}{\partial z} + \lambda \nabla \cdot \vec{v} \\ \tau_{rr} &= 2\mu_T \frac{\partial u_r}{\partial r} + \lambda \nabla \cdot \vec{v} \\ \tau_{\theta\theta} &= 2\mu_T \left(\frac{1}{r} \frac{\partial u_\theta}{\partial \theta} + \frac{u_r}{r} \right) + \lambda \nabla \cdot \vec{v} \\ \tau_{r\theta} &= \tau_{\theta r} = \mu_T \left[r \frac{\partial}{\partial r} \left(\frac{u_\theta}{r} \right) + \frac{1}{r} \frac{\partial u_r}{\partial \theta} \right] \\ \tau_{\theta z} &= \tau_{z\theta} = \mu_T \left[\frac{\partial u_\theta}{\partial z} + \frac{1}{r} \frac{\partial u_z}{\partial \theta} \right] \\ \tau_{zr} &= \tau_{rz} = \mu_T \left[\frac{\partial u_z}{\partial r} + \frac{\partial u_r}{\partial z} \right] \end{aligned} \quad (6)$$

$$\nabla \cdot \vec{V} = \frac{1}{r} \frac{\partial(ru_r)}{\partial r} + \frac{1}{r} \frac{\partial u_\theta}{\partial \theta} + \frac{\partial u_z}{\partial z}$$

$$\lambda = -\frac{2}{3} \mu_T \quad (7)$$

Heat flux terms are defined.

$$q_z = -k_T \frac{\partial T}{\partial z}, \quad q_r = -k_T \frac{\partial T}{\partial r}, \quad q_\theta = -\frac{k_T}{r} \frac{\partial T}{\partial \theta} \quad (8)$$

And now total viscosity and thermal conductivity coefficients are given.

$$\mu_T = \mu + \mu_{turb}, \quad k_T = k + k_{turb} \quad (9)$$

The axisymmetric equations are determined by setting θ derivatives to zero and multiplying the equations by $2\pi r$ and adjusting the areas and volumes to account for 360° rotation about the x -axis. Axisymmetric flows are computed in the x - y plane.

$$\frac{\partial(2\pi r Q)}{\partial t} + \frac{\partial(2\pi r E)}{\partial z} + \frac{\partial(2\pi r F)}{\partial r} + 2\pi r H$$

$$= \frac{\partial(2\pi r E_v)}{\partial z} + \frac{\partial(2\pi r F_v)}{\partial r} + 2\pi r H_v \quad (10)$$

Finally, the finite volume form of the 2D/axisymmetric equations.

$$\frac{d}{dt} \int Q dS' + \int [(E - E_v) \hat{n}_x + (F - F_v) \hat{n}_y] dl'$$

$$= - \int (H - H_v) dS'_y = - \int r(H - H_v) dl'_y \quad (11)$$

$$dS' = 2\pi r dS, \quad dl' = 2\pi r dl \quad (12)$$

A.2. Chemistry model

Details of the chemistry model are given in [29] and summarized here (Table 1).

Table 1

The 7-species, 8-reaction system used in the model, with associated forward Arrhenius rate constants where the reaction rate from the Arrhenius equation, k , has units $\text{cm}^3/\text{mole}\cdot\text{s}$.

Reactions	A	B	C
1 $\text{H}_2 + \text{M} \rightarrow \text{H} + \text{H} + \text{M}$	5.5×10^{18}	-1.0	51987
2 $\text{O}_2 + \text{M} \rightarrow \text{O} + \text{O} + \text{M}$	7.2×10^{18}	-1.0	59340
3 $\text{H}_2\text{O} + \text{M} \rightarrow \text{OH} + \text{H} + \text{M}$	5.2×10^{21}	-1.5	59386
4 $\text{OH} + \text{M} \rightarrow \text{O} + \text{H} + \text{M}$	8.5×10^{18}	-1.0	50830
5 $\text{H}_2\text{O} + \text{O} \rightarrow \text{OH} + \text{OH}$	5.8×10^{13}	0	9059
6 $\text{H}_2\text{O} + \text{H} \rightarrow \text{OH} + \text{H}_2$	8.4×10^{13}	0	10116
7 $\text{O}_2 + \text{H} \rightarrow \text{OH} + \text{O}$	2.2×10^{14}	0	8455
8 $\text{H}_2 + \text{O} \rightarrow \text{OH} + \text{H}$	7.5×10^{13}	0	5586

References

- [1] E. Oran, V. Gamezo, Origins of the deflagration-to-detonation transition in gas-phase combustion, *Combust. Flame* 148 (2007) 4–47.
- [2] G. Ciccarelli, S. Dorofeev, Flame acceleration and transition to detonation in ducts, *Prog. Energy Combust. Sci.* 34 (2008) 499–550.
- [3] Y. Zeldovich, V. Librovich, G. Makhviladze, G. Sivashinskii, On the onset of detonation in a nonuniformly heated gas, *J. Appl. Mech. Tech. Phys.* 11 (1970) 264–270.
- [4] V. Gamezo, T. Ogawa, E. Oran, Numerical simulations of flame propagation and DDT in obstructed channels filled with hydrogen-air mixture, *Proc. Combust. Inst.* 31 (2007) 2463–2471.
- [5] G. Goodwin, R. Houim, E. Oran, Effect of decreasing blockage ratio on DDT in small channels with obstacles, *Combust. Flame* 173 (2016) 16–26.
- [6] J. Lee, I. Moen, The mechanism of transition from deflagration to detonation in vapor cloud explosions, *Prog. Energy Combust. Sci.* 6 (1980) 359–389.
- [7] A. Teodorczyk, P. Drobniak, A. Dabkowski, Fast turbulent deflagration and DDT of hydrogen-air mixtures in small obstructed channel, *Int. J. Hydrogen Energy* 34 (2009) 5887–5893.
- [8] A. Heidari, J.X. Wen, Numerical simulation of flame acceleration and deflagration to detonation transition in hydrogen-air mixture, *Int. J. Hydrogen Energy* 39 (2014) 21317–21327.
- [9] D. Chapin, A study of deflagration to detonation transition in pulsed detonation engine, Georgia Institute of Technology, 2005 Master's thesis.
- [10] A.V. Gaathaug, K. Vaagsaether, D. Bjerketvedt, Experimental and numerical investigation of DDT in hydrogen air behind a single obstacle, *Int. J. Hydrogen Energy* 37 (2012) 17606–17615.
- [11] A. Teodorczyk, J. Lee, R. Knystautas, The structure of fast turbulent flames in very rough, obstacle-filled channels, *Symp. (Int.) Combust.* 23 (1990) 735–741.
- [12] A. Heidari, J.X. Wen, Flame acceleration and transition from deflagration to detonation in hydrogen explosions, *Int. J. Hydrogen Energy* 39 (2014) 6184–6200.
- [13] V. Gamezo, T. Ogawa, E. Oran, Flame acceleration and DDT in channels with obstacles: effect of obstacle spacing, *Combust. Flame* 155 (2008) 302–315.
- [14] G. Goodwin, R. Houim, E. Oran, Shock transition to detonation in channels with obstacles, *Proc. Combust. Inst.* 36 (2017) 2717–2724.
- [15] T. Ogawa, V. Gamezo, E. Oran, Flame acceleration and transition to detonation in an array of square obstacles, *J. Loss Prev. Process Ind.* 26 (2013a) 355–362.
- [16] T. Ogawa, E. Oran, V. Gamezo, Numerical study on flame acceleration and DDT in an inclined array of cylinders using an amr technique, *Comput. Fluids* 85 (2013b) 63–70.
- [17] D. Kessler, V. Gamezo, E. Oran, Simulations of flame acceleration and deflagration-to-detonation transitions in methane-air systems, *Combust. Flame* 157 (2010) 2063–2077.
- [18] M. Ivanov, A. Kiverin, I. Yakovenko, M. Liberman, Hydrogen-oxygen flame acceleration and deflagration-to-detonation transition in three-dimensional rectangular channels with no-slip walls, *Int. J. Hydrogen Energy* 38 (2013) 16427–16440.
- [19] M. Liberman, M. Ivanov, A. Kiverin, M. Kuznetsov, A. Chukalovsky, T. Rakhimova, Deflagration-to-detonation transition in highly reactive combustible mixtures, *Acta Astronaut.* 67 (2010) 688–701.
- [20] M. Ivanov, A. Kiverin, M. Liberman, Hydrogen-oxygen flame acceleration and transition to detonation in channels with no-slip walls for a detailed chemical reaction model, *Phys. Rev. E* 83 (2011a) 056313.
- [21] M. Ivanov, A. Kiverin, M. Liberman, Flame acceleration and DDT of hydrogen-oxygen gaseous mixtures in channels with no-slip walls, *Int. J. Hydrogen Energy* 36 (2011b) 7714–7727.
- [22] M. Kuznetsov, V. Alekseev, I. Matsukov, S. Dorofeev, DDT in smooth tube filled with a hydrogen-oxygen mixture, *Shock Waves* 14 (2005) 205–215.
- [23] M. Kuznetsov, M. Liberman, I. Matsukov, Experimental study of the preheat zone formation and deflagration to detonation transition, *Combust. Sci. Technol.* 182 (2010) 1628–1644.
- [24] M. Wu, M. Burke, S. Son, R. Yetter, Flame acceleration and the transition to detonation of stoichiometric ethylene/oxygen in microscale tubes, *Proc. Combust. Inst.* 31 (2007) 2429–2436.
- [25] D. Valiev, V. Bychkov, V. Akkerman, C. Law, L.-E. Eriksson, Flame acceleration in channels with obstacles in the deflagration-to-detonation transition, *Combust. Flame* 157 (2010) 1012–1021.
- [26] E. Luke, T. George, Loci: a rule-based framework for parallel multidisciplinary simulation synthesis, *J. Funct. Prog.* 15 (2005) 477–502.
- [27] E. Luke, On robust and accurate arbitrary polytope CFD solvers, 18th AIAA Computational Fluid Dynamics Conference, June 25–28 (2007), Miami, FL. AIAA Paper 2007-3956, doi:10.2514/6.2007-3956.
- [28] Pointwise, Inc., <https://www.pointwise.com/>.
- [29] J. Evans, C. Schexnayder, Influence of chemical kinetics and unmixedness on burning in supersonic hydrogen flames, *AIAA J.* 18 (1980) 188–193.
- [30] E. Luke, X. Tong, J. Wu, P. Cinnella, R. Chamberlain, CHEM 3.3: a finite-rate viscous chemistry solver – the user guide, 2014.
- [31] D. Allgood, Development of detonation modeling capabilities for rocket test facilities: hydrogen-oxygen-nitrogen mixtures, NASA Technical Report NASA/TP-2016-219220, NASA Technical Reports Server (NTRS), Washington, D.C., 2016.
- [32] H. Xiao, Q. Duan, J. Sun, Premixed flame propagation in hydrogen explosions, *Renew. Sustain. Energy Rev.* 81 (2018) 1988–2001.
- [33] H. Xiao, R. Houim, E. Oran, Formation and evolution of distorted tulip flames, *Combust. Flame* 162 (2015) 4084–4101.
- [34] K. Jin, Q. Duan, K. Liew, Z. Peng, L. Gong, J. Sun, Experimental study on a comparison of typical premixed combustible gas-air flame propagation in a horizontal rectangular closed duct, *J. Hazard. Mater.* 327 (2017) 116–126.
- [35] H. Xiao, J. Sun, P. Chen, Experimental and numerical study of premixed hydrogen/air flame propagating in a combustion chamber, *J. Hazard. Mater.* 268 (2014) 132–139.
- [36] A. Khokhlov, E. Oran, Numerical simulation of detonation initiation in a flame brush: the role of hot spots, *Combust. Flame* 119 (1999) 400–416.